Synthesis and characterization of nanoscale composite particles formed by 2D layers of Cu-Fe sulfide and Mg-based hydroxide

Yuri L. Mikhlin[a*], Roman V. Borisov[a,c], Sergey A. Vorobyev[a], Yevgeny V. Tomashevich[a], Alexander S. Romanchenko[a], Maxim N. Likhatski[a], Anton A. Karacharov[a], Oleg A. Bayukov[b], Yuriy V. Knyazev[b], Dmitriy A. Velikanov[b], Sergey M. Zharkov[b,c], Alexander S. Krylov[b], Svetlana N. Krylova[b], Ivan V. Nemtsev[b,c,d]

[a] *Institute of Chemistry and Chemical Technology, Krasnoyarsk Science Center of the Siberian Branch of the Russian Academy of sciences, Akademgorodok, 50/24, Krasnoyarsk, 660036, Russia*
[b] *Kirensky Institute of Physics, Krasnoyarsk Science Center of the Siberian Branch of the Russian Academy of sciences, Akademgorodok 50/38, Krasnoyarsk, 660036, Russia*
[c] *Siberian Federal University, Svobodny av. 79, Krasnoyarsk, 660041, Russia*
[d] *Federal Research Center "Krasnoyarsk Science Center of the Siberian Branch of the Russian Academy of sciences", Akademgorodok, 50, Krasnoyarsk, 660036, Russia*

* corresponding author, e-mail: yumikh@icct.ru

Abstract

We introduce here a multifunctional material composed of alternating atomic sulfide sheets close to $CuFeS_2$ and Mg-based hydroxide ones (valleriite), which are assembled due to their electric charges of opposite sign. Valleriite particles of 50-200 nm in the lateral size and 10-20 nm thick were synthesized via a simple hydrothermal pathway using various concentrations of precursors and dopants, and examined with XRD, TEM, EDS, X-ray photoelectron spectroscopy, reflection electron energy loss spectroscopy (REELS), Mössbauer, Raman and UV-vis-NIR spectroscopies, magnetic, dynamic light scattering, zeta potential measurements. The electronic, magnetic and optical characteristics are found to be critically dependent of the charge (electron density) at the narrow-gap sulfide layers containing Cu^+ and Fe^{3+} cations, and can be tuned via the composition of hydroxide part. Particularly, substitution of Mg^{2+} with Al^{3+} increases the negative charge of the hydroxide layers and reduces the content of Fe^{3+}-OH centers (10-45% of total iron); the effects of Cr and Co dopants entering both layers are more complicated. Mössbauer doublets of paramagnetic Fe^{3+} detected at room temperature transform to several Zeeman sextets at 4.2 K; the hyperfine fields up to 500 kOe and complex magnetic behavior, but not pure paramagnetism or antiferromagnetism, were observed for valleriites with the higher positive charge of the sulfide sheets, probably due to the depopulation of the minority-spin 3d states of S-bonded Fe^{3+} ions. Aqueous colloids of valleriite show optical absorption at 500 - 750 nm, which, along with the peaks at the same energies in REELS, may arise due to quasi-static dielectric resonance involving the vacant Fe 3d band and being dependent on the composition of both layers too. These and other findings call attention to the of valleriites as a new rich family of 2D materials for a variety of potential applications.

Keywords: two-dimensional metal sulfide, sulfide-hydroxide composite, valleriite, aqueous colloids, magnetism, optical absorption

1. Introduction

Two-dimensional (2D) materials attract much attention [1-13] owing to the large specific surface area and a wide spectrum of unique physical and chemical properties, which are of vivid interest for electronics, spintronics, energetics, sensors, photonics, catalysis, biomedical and other applications. There are known few families of 2D materials and composites beyond graphene. Transition metal dichalcogenides constructed by two-dimensional sheets stacked by van der Waals (vdW) forces, for example, MoS_2 and related substances with metallic conductivity, are rather inert because of a low density of active centers and should be modified for many applications [11-19]. Other metal chalcogenides, including ternary [14,16], incline to undesirable oxidation and corrosion. A variety of electronic, magnetic, optical properties of Mo and W dichalcogenides, as well as MXenes with $Ti_3C_2T_x$ as a typical representative (T_x is the surface terminal groups O, OH, S, F) [8-10], are restricted by the metal nature. Layered double hydroxides (LDH) are based on the structure of brucite $Mg(OH)_2$ where Mg^{2+} is partially substituted by, for example, Al^{3+} cations (the nature of both cations can be changed), and the electric charge is balanced with anions located between the layers, often together with water molecules. The applications of LDHs are largely related with their ability to host a wide range of intercalates and other chemical properties, while electronic and magnetic characteristics of these mainly dielectric materials have received much less attention.

We propose here a multifunctional 2D composite constructed by alternating quasi-atomic sulfide layers close to $CuFeS_2$ and metal hydroxide layers based on $Mg(OH)_2$ (Fig. 1). The natural prototype of this material is mineral valleriite [20-30] that remains poorly explored and uninvolved in commercial processing [28,29]. The minerals usually contain Al and Fe cations replacing Mg in the brucite-like sheets; for instance, Hughes et al. [30] have reported the composition of valleriites ranged from $[CuFeS_2]\cdot 1.67[Mg_{0.70}Al_{0.30}(OH)_2]$ to $[Cu_{1.30}Fe_{0.70}S_2]\cdot 1.35[Mg_{0.74}Al_{0.26}(OH)_2]$. Minerals of the valleriite group [31-34] with iron dominance in hydroxide layers (mineral ferrovalleriite) [31,32] or chromium instead of iron in hydroxide and sulfide sheets [33], or FeS layers in place of $CuFeS_2$ (tochilinite) [24,27,35,36] were discovered too. Valleriite is known [20,24,25,30] to crystallize in a hexagonal lattice with the sulfide sublattice being rhombohedral (space group $R\bar{3}m$ with hexagonal axes a = 0.3792 nm and c = 0.341 nm) and the hydroxide one having hexagonal lattice (space group $P\bar{3}m1$, a = 0.307 nm and c = 1.137 nm). Two atomic S layers form tetrahedral sites occupied, probably statistically, by Cu^+ and Fe^{3+} cations, whereas metals are in octahedral coordination with OH^- anions in the hydroxide part (Fig. 1). Al^{3+} cations located in Mg^{2+} sites have been suggested to induce a positive electric charge of the brucite-type layer so the sulfide sheets are charged negatively and stacked by the opposite electric charges [30]. Iron preferentially occurs as Fe^{3+}-S centers but Fe^{2+}-S, Fe^{3+}-OH and Fe^{2+}-OH species may exist too [26,35-37]. Recently we performed X-ray absorption, photoelectron (XPS), Mössbauer spectroscopy and magnetic investigation of natural valleriite samples [38,39] and found, in particular, that the Mössbauer signals of paramagnetic Fe^{3+} transform to a series of Zeeman sextets below 70 K instead of antiferromagnetic ordering in bulk chalcopyrite $CuFeS_2$ and other Cu-Fe sulfides [40]. Exact nature of the Fe species and many basic properties of valleriites are still indeterminate due to the complexity of mineral assemblages.

Attempts to synthesize valleriite via thermal sintering or hydrothermal route have been undertaken [30,35-37,41,42] but produced mixtures of valleriite (less than 50%) with chalcopyrite, magnetite and other by-products. In recent years, a number of similar composites with the layered structure constructed by iron selenide and lithium-based hydroxides $(Li_{1-x}Fe_x)(OH)\cdot FeSe$ [43-47] have been prepared and studied as superconductors with the critical temperature T_c up to 40 K. Such materials as $[(Fe,Al)(OH)_2][FeSe]_{1.2}$ [48],

[$(Li_{0.8}Fe_{0.2})OH$]$Fe(S_{1-x}Se_x)$ [49], $(Na_xFe_{1-x})(OH)FeS$ [50] and intercalated iron chalcogenides [51] were also obtained in efforts, though unsuccessful yet, to enhance the T_c.

The aims of the current study were to develop a facile synthetic route to pure valleriites, including colloidal solutions and chemically modified materials (with Al, Si, Cr, Co, rare earth elements), and to elucidate their basic characteristics. The results obtained here highlight valleriite, $(Cu,Fe)S_2 \cdot n(Mg,Fe,Al)(OH)_2$, as a novel platform for preparation of multifunctional two-dimensional materials with tunable properties.

2. Materials and methods

2.1. Materials and synthetic procedures

Analytical grade commercial iron (II) sulfate $FeSO_4 \cdot 7H_2O$, copper sulfate $CuSO_4 \cdot 5H_2O$, sodium sulfide $Na_2S \cdot 9H_2O$, magnesium sulfate $MgSO_4 \cdot 7H_2O$, aluminum sulfate $Al_2(SO_4)_3 \cdot 18H_2O$, cobalt (II) chloride $CoCl_2 \cdot 6H_2O$, chromium (III) chloride $CrCl_3 \cdot 6H_2O$, lanthanum (III) chloride $LaCl_3 \cdot 7H_2O$, gadolinium (III) nitrate $Gd(NO_3)_3 \cdot 5H_2O$ and aqueous ammonia were used without further purification. Deionized water (Millipore Milli-Q grade) was utilized to prepare the reagent solutions, to wash the precipitates, etc. In a typical procedure, pre-determined quantities of Fe and Cu sulfates (e.g., 0.556 g and 0.50 g, respectively) were dissolved in a small water volume and freshly prepared 20% solution of Na_2S was slowly added under agitation, producing metal sulfide precipitates. Gelatinous sediments of magnesium hydroxide or its mixture with aluminum hydroxide were obtained by adding 25% aqueous ammonia to solutions of Mg and Al sulfates. This dispersion was transferred to the glass with Fe and Cu sulfides, pH was adjusted to 10-11 with aqueous ammonia, and the mixture was loaded into an in-home made stainless steel autoclave with Teflon liner [52] (Fig. S1, Supplementary material). The vessel (32 cm^3) was purged with Ar and sealed, rotated (8 rpm) at room temperature for about 1 h and then heated to 160 ºC using air thermostat. After heating (from 2 h to 100 h), the autoclave was cooled in air, and solid products were separated using centrifugation (CR4000, Centurion Scientific, UK) at 4000 Hz for 15 min. The precipitate was washed 4-5 times via re-dispersion in water and centrifugation. The residue was stored as a wet paste and dried in air at room temperature before examination. So, the process was performed using a large, 2-to-10-fold excess of sulfide anions, with excessive reagents rejected upon the centrifugation and washing. Totally, more than 50 specimens of valleriites with varying composition were successfully manufactured, as confirmed using XRD and XPS. Table 1 shows the designations and synthesis conditions for valleriite samples selected to present in this paper; the letters (a)-(i) are used to mark the specified samples throughout the article.

Table 1. Designations, atomic proportions of precursors, and time of heating under hydrothermal conditions (160 ºC) for selected valleriite samples

Sample index	Atomic proportions of precursors						Time (h)
	Fe	Cu	S	Mg	Al	Dopant	
a	2	1	10	2	-	-	33
b	2	1	14	2	2	-	33
c	2	2	15	1.5	1.5	-	50
d	2	2	14	2	0.5	-	25
e	1.8	2	14.8	1.5	1	Cr 0.2	50
f	1.5	2	14.8	1.5	1	Cr 0.5	50
g	1.8	2	14.8	1.5	1	Co 0.2	50
h	1.8	2	14.8	1.5	1	La 0.2	50
i	2	2	14	2	0.5	Si 1.0	32

To produce colloidal solutions, the residue (approximately 0.01 g) was dispersed in 50 mL of aqueous 2 mM solution of sodium dodecyl sulfate (SDS) (Merck) with ultrasonic treatment (22 kHz, 15 W/cm^2, 3 min) with a Volna-M source (Center of Ultrasound Technologies, Russia). Colored supernatants (sols) spontaneously formed in many cases after the centrifugation were diluted with water before exploration.

2.2. Characterization

X-ray powder diffraction patterns were obtained from air-dried powders using a PANalytical X'Pert Pro diffractometer with Cu Kα radiation.

Transmission electron microscopy (TEM) images, energy dispersive X-ray analysis (EDS) and selected area electron diffraction (SAED) patterns were collected with a JEM 2100 microscope (JEOL, Japan) operated at accelerating voltage of 200 kV. Particles were dispersed in ethanol before the experiment and a sol droplet was placed on a carbon coated Ni grid (Ted Pella Inc., USA) and allowed to dry at room temperature. Scanning electron microscopy (SEM), EDS and elemental mapping were made utilizing a Hitachi TM 3000 instrument operated at the acceleration voltage of 15 kV, equipped with a Bruker Quantax 70 analyzer.

X-ray photoelectron spectra were acquired with a SPECS instrument (SPECS GmbH, Germany) equipped with a PHOIBOS 150 MCD-9 analyzer operated at the pass energy of 20 eV for survey spectra and 10 eV for high-resolution spectra. Monochromatic Al Kα irradiation (1486.7 eV) of the X-ray tube was used for excitation. The pressure in an analytical chamber was in the range of 10^{-9} mbar. Solid samples were placed on sticky carbon tape; hydrosol droplets were dried on highly oriented pyrolytic graphite (HOPG). The atomic concentrations were obtained from the survey spectra. The high-resolution spectra were fitted with Gaussian-Lorentzian peak profiles after subtraction of the Shirley-type background. Spin-orbit splitting and an intensity ratio for S $2p_{3/2,1/2}$ doublet were assumed of 1.19 eV and 2:1, respectively. The Fe 2p spectra were fitted with two sets of multiplet lines (four narrow peaks and a wider satellite) [53] for Fe^{3+} cations bonded to hydroxide anions and to sulfide; possible contributions of Fe^{2+} were taken into consideration too. The energy splitting and relative intensities of lines within the sets were put at the values insignificantly different from those in [53] with the widths allowed to vary in the range of 10 rel. %, while the BE of the set as a whole were optimized, both for Fe^{3+}-O and Fe^{3+}-S species. CasaXPS software was applied for data processing. Electron energy loss spectra in the reflection mode (REELS) were collected using a STAIB electron gun incorporated in the SPECS instrument, with the width at half maximum (FWHM) of elastically reflected beam of 0.7 eV.

^{57}Fe Mössbauer spectra were measured in a transmission mode employing an MC-1104Em spectrometer (Cordon, Russia) with a ^{57}Co(Rh) source that was kept at room temperature, while the absorber (powdered valleriites about 3 mg/cm^2 of Fe in thickness) were either at 20 ºC or cooled down to liquid helium temperature (4.2 K) with a CFSG-311-MESS cryostat (Kriotreid Ltd, Russia). Isomer shifts (IS) are given relative to α-iron at room temperature. Probabilities P of quadrupole splitting P(QS) and magnetic hyperfine fields P(H) were first determined from the experimental spectra and were used to generate a model spectrum and then to fit the results by varying the complete set of parameters [54].

Magnetization of valleriite samples was measured using a superconducting quantum interference device (SQUID) magnetometer [55], typically with a magnetic field of 500 Oe in field cooled, FC, and zero field cooled, ZFC, regimes in the temperature range from 4.2 K to 290 K. The magnetic moment was also determined as a function of the magnetic field varied from 0 to 800 Oe.

Dynamic light scattering (DLS) and zeta potential measurements were performed using Zetasizer Nano ZS spectrometer (Malvern Instruments, UK) at scattering angle 173° in a polycarbonate cell with Pd electrodes at 25 ºC. UV−vis-NIR absorption spectra of hydrosols

were collected in the range 200 - 1400 nm in a thermostatic quartz cell with the optical path of 1 cm using a Shimadzu UV 3600 instrument.

3. Results

3.1. Morphology, phase and chemical composition

Figure 1 shows selected X-ray diffraction patterns and typical TEM micrographs of the reaction products. XRD, as well as electron diffraction, revealed reflections of valleriite, which are in agreement with the literature [20], as the only or predominant crystalline phase for the reaction mixtures contained atomic proportions of Fe/Cu of 1-2, Fe/Mg of about 1±0.25 and a big excess of sodium sulfide. Extra peaks at the diffraction patterns are very minor, if any, as, for example, the one of brucite $Mg(OH)_2$ near 2 theta of 18º (sample a). The XRD reflections of valleriite emerged within 2 h heating and became narrower as the reaction proceeds.

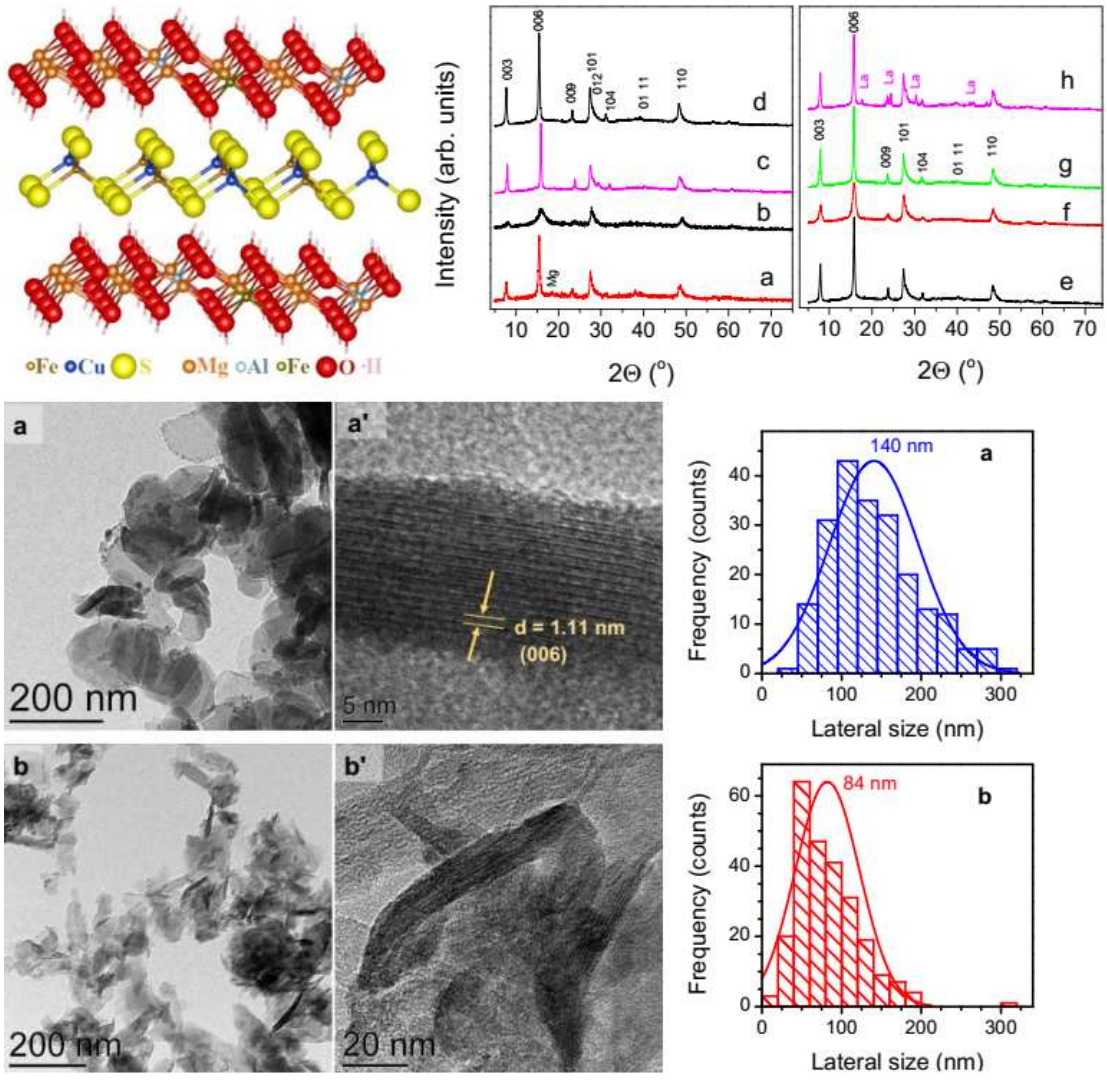

Fig. 1. Atomic structure of the Cu-Fe sulfide and $(Mg,Fe,Al)(OH)_2$ sheets in valleriite (slightly tilted for better view), X-ray diffraction patterns and representative TEM images and particle size distributions of valleriite samples synthesized (a) without Al, (b) with Al and (c, d) various initial ratios of Fe, Cu, Mg precursors. XRD data illustrate the effect of addition of (e, f) Cr, (g) Co and (h) La; reflections of Mg and La hydroxides are marked as Mg (a) and La (h). Please see Table 1 for sample preparation details.

TEM micrographs (additional images, selected area electron diffraction patterns and EDS data are given in Figs. S2-S4, Supplementary material) depict plain particles of 50-200 nm in the lateral size together with elongated ones with the width of 10-25 nm. The last entities are not nanorods but the same particles exposing their edges; this is obvious from the TEM images taken from tilted specimens (Fig. S2). TEM on the particle edge (a', b') revealed the interatomic distances of about 1.1 nm characteristic of the valleriite structure [20-25,39]. The particles are 10-20 layers thick, and both the lateral dimension and thickness depend on the starting composition of the reaction mixture. Particularly, the particles became smaller and less regular as Al was added, with no new phases emerged for the reaction ratio Al/Mg less than 1. XRD reflections widened (compare the samples a and b) and showed a reduction of the interplanar distance [006] and some other distortions of the hydroxide structure caused by smaller Al^{3+} cations. No additional phases were detected upon substitution of Fe with transition 3d metals (the contents of Co and Cr up to 30% of Fe were tested), whereas a large share of rare-earth metals (La, Gd), as well as Si, formed their own hydroxide phases (see Fig. 2, *h* as an example).

Table 2. Concentrations of elements (C and O are disregarded) in the products determined using EDS and XPS; see Table 1 for description of the samples

Sample	Concentrations (at.%)						
	Fe	Cu	S	Mg	Al	Na	Co
a	23.6	12.5	33.9	30.0	-		
XPS	12.7	8.3	37.8	41.2	-	-	
b	14.6	9.4	26.4	27.2	20.4	-	-
XPS	10.2	6.2	34.1	31.4	18.1	-	-
g	16.2	19.3	34.5	18.8	8.8	0.7	1.7
XPS	9.3	15.2	36.0	21.4	15.0	2.2	0.9

The chemical composition of several valleriite samples is given in Table 2 and Figs. S3, S4. It generally falls within the range reported in the literature [27,30] and substantially differs from the initial proportions of precursors used in the synthesis since excessive amounts of S, Al, Na, partially Fe and Mg are rejected by means of the centrifugation and washing. Nevertheless, the solid product composition can be tuned by varying the concentrations of reagents; in particular, valleriites have a deficit of Fe regarding $CuFeS_2$ for the initial proportion Fe/Cu ≈1 (b, g), and excess of Fe for the proportion Fe/Cu =2 (a), although the non-stoichiometry is not so big. The samples may contain small quantities of Na^+ cations and sulfate anions uptaken by the valleriite surfaces (the next section). EDS elemental maps (Fig. S3, S4) display uniform spatial distributions of elements, including dopants.

3.2 XPS and REELS

Surface concentrations of elements derived from XPS and also shown in Table 2 are in reasonable agreement with the EDS data, albeit the deficit of iron and excess of sulfur are somewhat larger, probably, owing to oxidation of the outer layers probed by the surface-sensitive XPS. The spectra of copper are essentially the same for all the samples, with the major Cu $2p_{3/2}$ component (more than 80% of the total peak intensity) at the binding energy (BE) of 932.5 eV ± 0.1 eV, negligible shake-up satellites at 944-948 eV and Cu L_3MM Auger peak at the kinetic energy of 917.0 eV being characteristic of Cu^+ cations bonded to sulfur [38,56-59]. The Cu $2p_{3/2}$ maxima are slightly broadened at higher BEs that is typical for many copper sulfides due to minor Cu^{2+}/Cu^+-O species and/or shake-off satellites [56,57].

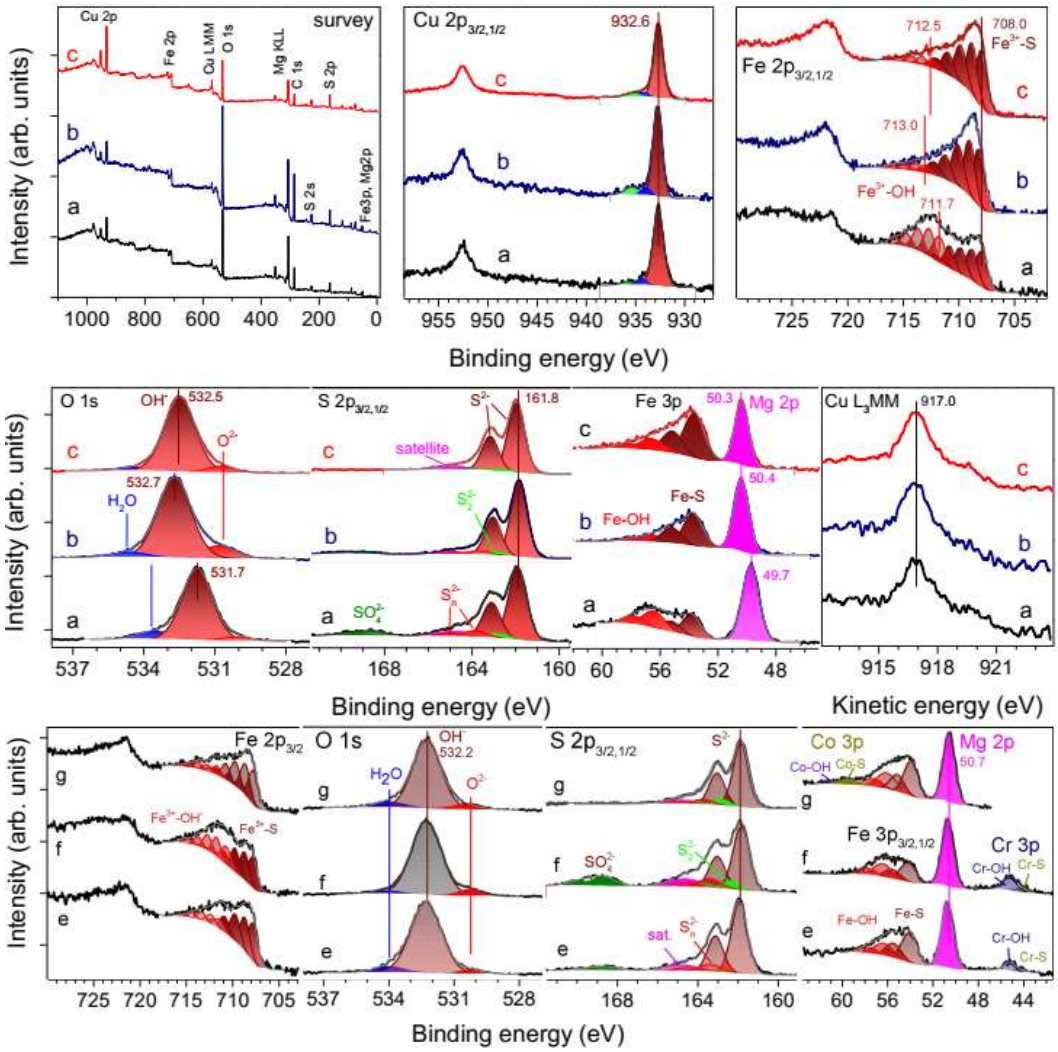

Fig. 2. X-ray photoelectron spectra of valleriites synthesized with different proportions of Fe and Cu precursors without Al (a) and with Al (b, c, e, f, g) and also (lower panel) doped with (e), (f) Cr and (g) Co. The designations a, b, etc. correspond to the samples listed in Table 1 and 2; the spectra of sample (d), which are similar to those of sample (c), are omitted.

The Fe $2p_{3/2}$ bands can be fitted using two five-line multiplet sets [53] with the first peaks at 708 eV and 711-712 eV attributable to Fe^{3+} cations bonded to sulfide and hydroxide anions, respectively [53,59,60]. The position of the Fe-S lines is almost the same for all valleriites while the BEs of Fe^{3+}-OH component can shift by more than 1 eV concurrently with the bands of Mg 2p and O 1s as described below. This means, among other things, that these Fe atoms occur in the hydroxide layer of valleriite but not in a separate phase. The fitting is not entirely unambiguous, and minor Fe^{2+}-S and Fe^{2+}-O species may be missed. The Fe 3p spectra, which don't have the complicated multiplet structure and characterize somewhat thicker layers due to higher kinetic energies (lower BEs) of photoelectrons, are composed of wide maxima and are inconclusive in terms of possible marginal components too. Anyway, both the Fe 2p and 3p spectra demonstrate that from 55% to 90% of iron atoms are located in the sulfide sheets as predominant Fe^{3+} species, and the rest are in the brucite-like layers. It is important to note that the concentration of OH-bonded Fe reduces with addition of Al, a decrease of the initial precursor proportion Fe/Cu, and, in a lesser extent, with increasing reaction time.

The main S 2p doublet with the BE of S $2p_{3/2}$ peak at 161.7±0.1 eV in amounts up to 80% of the total intensity slightly decreases in case of a large share of Fe-O species, whereas the small components at about 162.5 eV and 163.5 eV from di- and polysulfide species [58-

60], respectively, grow. The S 2p spectra are better fitted using an additional broad maximum centered near 164.5 eV that appears to be a satellite related to electron transfer to vacant Fe 3d states [56-60]. Up to 10% of sulfur is present as sulfate anions adsorbed from the solution. Therefore, the sulfide part of valleriite is often depleted in Fe that could transfer to hydroxide sheets and then to the environment from the near-surface layers, promoting S-S bonding.

As the content of Fe in the hydroxide part is diminished by adding the Al modifier in the synthesis, the BEs of Mg 2p, O 1s and Fe^{3+}-OH bands increase by ~1 eV due to a shift of the Fermi level toward a higher energy in the brucite-like sheets (see Fig. 3 for explanation) rather than changes of the chemical state of elements. The O 1s spectra, however, show, in addition to the major signal of OH^- groups shifted from 531.5 eV to ~532.5 eV, an increased contribution from O^{2-} species at a BE of ~530.5 eV. These findings suggest a more negative, or less positive, charge of the Al-bearing hydroxide layers owing to distortions of the hydroxide structure via replacement of Mg^{2+} and Fe^{3+} cations by smaller Al^{3+} cations and partial transformation of OH^- into O^{2-} anions through a release of protons.

XPS of Cr- and Co-doped samples determined that about 80% of Cr^{3+} cations enter hydroxide layers (Cr 3p spectra of the samples *e*, *f* in the lower wright-hand panel); this also results in increasing concentration of Fe^{3+}-OH species. Two thirds of cobalt go into sulfide sheets (spectra *g*), and 80% of Fe remains S-bonded, at least for the moderate concentrations of the dopant used (Table 1). Minor quantities of rare earth metals and Si, which mainly form separate hydroxide phases, are not distinguish by XPS.

Figure 3 shows electron energy loss spectra measured in the reflection mode (REELS), aligned to zero energy loss and normalized by the intensity of the reflected elastic peak. The spectra acquired using the primary electron beam energy from 3 000 eV to 300 eV, and so the probing depths from about 5 nm to 1 nm, are generally similar, implying insignificant changes with the depth. The energy band gap (E_g) can be determined from the REELS spectra by approximating the slope of maxima by a straight line and assigning E_g to values at the intersection with the energy axis [61]. The two linear plots may correspond to two band gap energies of 0.25 ± 0.2 eV in the sulfide sheets and 4.2± 0.5 eV, tentatively attributed to the fundamental gap in the sulfide and/or hydroxide parts. Although the approach is disputable for narrow-gap semiconductors, the first E_g value satisfactorily complies with the optical band gap (see Fig. 6) and with the gap in chalcopyrite, $CuFeS_2$, of about 0.5 eV between the valence band (VB) and the “intermediate” empty Fe 3d band [56,58-60]. Furthermore, the REELS spectra exhibit a distinct maximum with the energy loss of ~2.1 eV and ~2.5 eV for the samples synthesized without (a) and with Al modifier (b), respectively. The energies are again in agreement with the optical UV-vis-NIR absorption maxima.

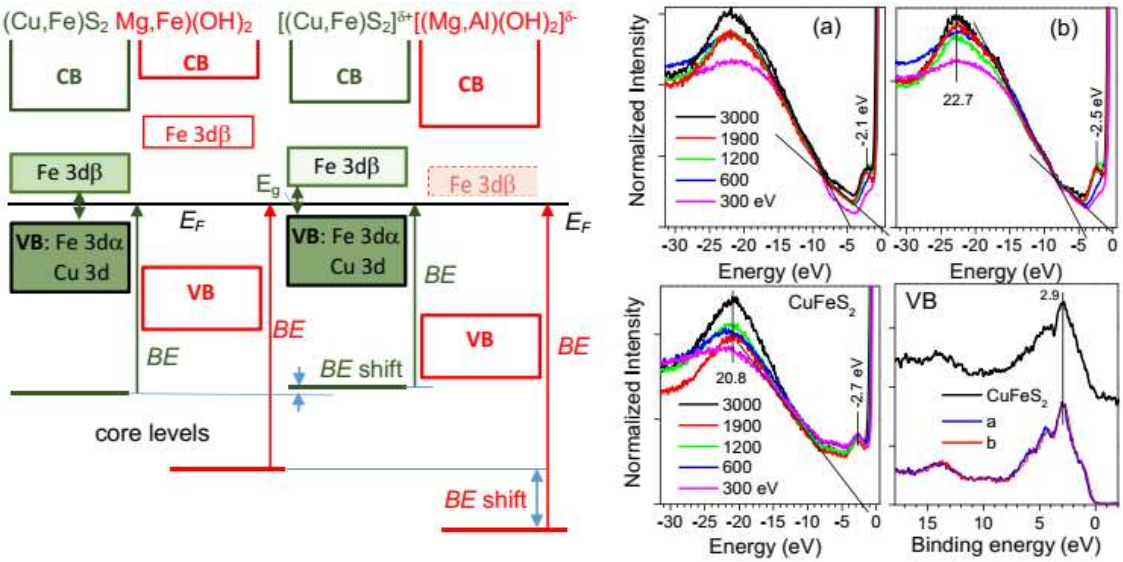

Fig. 3. Simplified band structure and BEs for Al-free and Al-doped valleriite; majority- and minority-spin Fe 3d states are marked with indexes α and β, respectively. Right panels show reflection electron energy loss spectra and XPS spectra of the valence band (VB) of vallerite (a) without and (b) with Al (Table 1), in comparison with the spectra of bulk chalcopyrite $CuFeS_2$. REELS was measured using varying energy of the incident electron beam marked in the plots.

It is instructive to compare the REELS and X-ray photoelectron spectra of the valence band (VB) of valleriites with those of chalcopyrite. The plasmon maximum of chalcopyrite has a lower energy of 20.8 eV vs. 22.7 eV in valleriites due to the smaller density of valence electrons and diverse dielectric properties, which are not considered here. The band gap width of ~2 eV as determined from the REELS of chalcopyrite is unreliable since the intensity onset is uncertain. The VB spectra reflecting the total density-of-states (DOS) are similar for both compounds as the main contribution is due to Cu 3d states peaked at 2.9 eV below the VB edge; small differences are observed near the VB top and at BEs of 4-5 eV where the density of Fe 3d states is significant. The position of the REELS feature at 2.7 eV is close the optical absorption maximum (about 500 nm) found for chalcopyrite quantum dots [73-76] as well as to the DOS maximum, by contrast to valleriites (2.1-2.5 eV vs 2.9 eV). It is noteworthy that REELS is insensitive, in difference to photoelectron spectra, to the Fermi energy position and electrostatic charging [61].

3.3. Mössbauer spectroscopy and magnetic measurements

^{57}Fe Mössbauer spectra (Fig. 4, Table S1) of the valleriites free of impurity phases shed new light onto the state of iron in comparison with the previous work on natural mineral assemblages and contaminated synthetic samples [26,35-37,39]. The asymmetric central signals observed at room-temperature can be fitted using 2 or 3 doublets with the isomeric shift (IS) of 0.34±0.03 mm/s and quadrupole splitting (QS) of 0.55±0.06 mm/s, and with IS = 0.4±0.05 mm/s and QS = 1.1±0.1 mm/s (Fig. 4, a-c), which should be assigned, from comparison their intensities with the XPS spectra (Fig. 2), to paramagnetic Fe^{3+} centers in tetrahedral coordination with S and octahedral coordination with OH^- groups, respectively. The spectra from the samples (a, b) prepared with excessive Fe precursor (i. e., Fe/Cu=2) are better fitted by using additional weak signals with a small or zero QS, which may be due to minor low-spin Fe^{2+} centers. The spectra of the samples prepared with Cr, Co, La dopants (the last two are not shown in Fig. 4) can be fitted using an additional doublet with QS > 1.2 mm/s possibly from Fe centers irregularly surrounded by different cations.

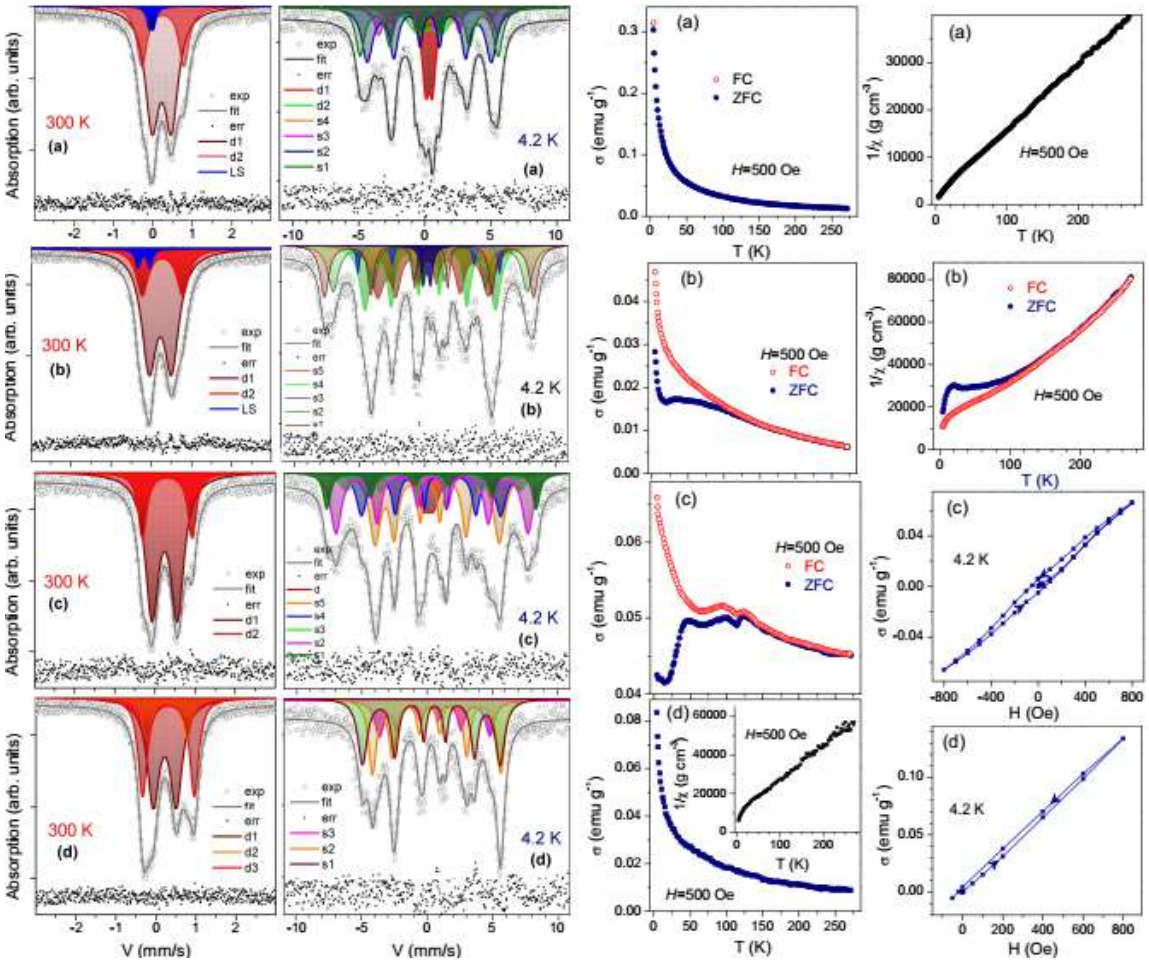

Fig. 4. Mössbauer spectra, temperature (FC and ZFC) and field dependences (hysteresis loops at 4.2 K) of magnetization and reciprocal susceptibility 1/χ of valleriites containing (a) no Al, (b), (c) with Al and (d) Cr-doped. The Mössbauer spectra were measured at room temperature (left panels) and 4.2 K; the points below the spectra are differences between the experimental results and fitted curves (colored lines). The designations (a), (b), (c), (d) correspond to the samples a, b, c, e, respectively, listed in Table 1. The best fit parameters for these and additional samples are given in Table S1.

The spectra collected at 4.2 K consist of a series of Zeeman sextets and minor doublets, with isomer shifts of the sextets ranged from 0.45 to 0.6 mm/s. The relative intensities of the sextets with negative or small QS approaching ~ 0 mm/s correlate with those of Fe^{3+}-S doublets at 300 K, whereas the ones with QS > 1 mm/s are likely due to Fe^{3+} in hydroxide sheets. A similar decrease of the quadrupole splitting to almost zero has been observed for the antiferromagnetic phase of bornite Cu_5FeS_4 below the Neel temperature (about 65 K) [40]. The emergence of several sextets means transition from the paramagnetic state to that with few distinct magnetically nonequivalent Fe positions in the 2D layers. The hyperfine fields H as high as ~500 kOe appear to relate with Fe sites in the sulfide sheets of Al-containing valleriites (samples b, c), and are absent in the samples with large concentrations of Fe-OH centers, including Cr- (spectra *d*) and Ln-doped materials, although their Mössbauer parameters somewhat differ (Table S1).

Typical temperature dependences of magnetization of valleriite samples exhibit almost coinciding pure paramagnetic FC and ZFC curves for the sample (a) with no Al and larger content of Fe in hydroxide layers. The more complicated behavior of Al-doped valleriites (b)

and (c), exhibiting the internal magnetic fields of 400-500 kOe in the Mössbauer spectra, may be interpreted in terms of paramagnetic, superparamagnetic and also minor ferromagnetic contributions [62-64] below ~120 K. Bulk antiferromagnetism that is characteristic of Cu-Fe sulfides ($CuFeS_2$, Cu_5FeS_4) [40,65] is not observed, possibly because of the strong paramagnetic signal, but local antiferromagnetic interactions cannot be ruled out. Valleriite doped with Cr (Fig. 4, *d*) is mainly paramagnetic but shows small ferromagnetic features (a drop of the reciprocal magnetic susceptibility $1/\chi$ and a hysteresis loop) below 20 K, which may be due to Cr centers.

As a first approximation, the correlations between the charge of the layers and relative content of Fe in the hydroxide part, high internal hyperfine fields and magnetic properties can be rationalized in terms of a larger negative charge of the hydroxide sheets and, correspondingly, a higher positive charge on the sulfide layers for Al-doped valleriites. The narrow gap (Fig. 3) between the VB and the empty "intermediate" band formed preferentially by minority-spin Fe 3d states suggests a relatively big number of the minority-spin electrons. The total electron density in the sulfide layers decreases mainly at the expense of these electrons, and iron becomes closer to pure high-spin Fe^{3+} ionic state with the hyperfine field at the Fe^{3+}-S sites approaching the characteristic value of ~500 kOe. The existence of several sextets with varying hyperfine fields at low temperatures are indicative of a few Fe centers both in sulfide and hydroxide sheets, the exact nature of which has still to be specified. Thus, the Mössbauer and magnetic measurements unveil interesting spin effects related with the charge of 2D layers, which require further investigation and open opportunities for engineering low-dimensional magnetic and spintronic materials.

3.4. Raman spectroscopy

Raman spectroscopy is an important tool for characterization of 2D materials that it sensitive to their atomic and electronic structures, number of layers and so forth [66]. Fig. 7 compares the Raman spectra of synthetic vallerriites having excess of Fe without (a) and with Al (b), and so high and low relatively contents of Fe in hydroxide layers, and the sample (c) with total deficit of Fe (please consult Table 1 for details), with natural valleriite [67] and chalcopyrite $CuFeS_2$ [68-71]. The spectrum of bulk chalcopyrite comprises of the main peak at 292 cm^{-1} and smaller ones at 315-380 cm^{-1}, which arise from a symmetric anion-only vibration (A_1 mode) [69,71] and Fe-S bond vibrations (B_2/E modes), respectively; the weaker feature near ~270 cm^{-1} is likely due to the Cu-S bond (B_2 mode) [69-71].

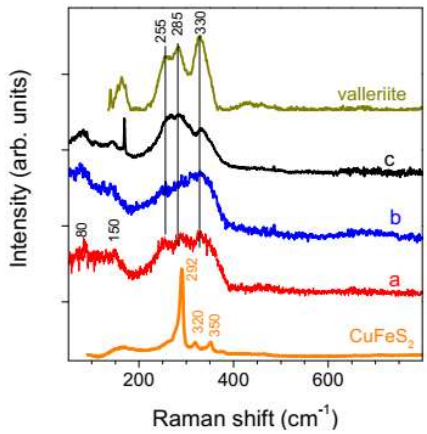

Fig. 5. Raman spectra of valleriites synthesized with (a) no Al and an excess of Fe (the initial atomic ratio of precursors Fe/Cu =2), (b) with Al and Fe/Cu =2, (c) with Al and the ratio of Fe/Cu=1, corresponding to the synthetic samples (a), (b) and (c) listed in Table 1, natural

valleriite [67] and chalcopyrite $CuFeS_2$ [68]. Narrow peak at ~170 cm^{-1} in the plot (c) is artefact due to laser harmonics.

The spectra of valleriites are composed of three intense maxima at about 255, 290 and 330 cm^{-1}, and weaker ones at 80 and 140 cm^{-1}, whose positions only slightly vary for the synthetic flakes and the bulk mineral of different composition but the relative intensities change considerably. Similar to chalcopyrite, the central peak at 290-295 cm^{-1} appears to be due to sulfur-only vibrations, which are almost independent on cations [71], but the relative intensities of other maxima are much larger for layered valleriite than chalcopyrite. The assignment of these vibrations to Cu-S (~255 cm^{-1}) and Fe-S bonds (330 cm^{-1}), respectively [69], agree with a higher intensity of the first peak for the sample (c) with the Cu-enriched sulfide layers (Table 2). So, Raman spectroscopy can provide information on the composition and structure of the sulfide part; unfortunately, weak scattering from hydroxide sheets was practically undetectable in these experiments.

3.5. Colloidal solutions

The hydrosols spontaneously formed during washing of valleriite and those produced by ultrasonic treatment of the residue in 2 mM SDS solutions demonstrate clear differences between the particles synthesized without and with Al in hydroxide layers, more pronounced for the surfactant-free colloids. The hydrodynamic diameters D_h (Fig. 6, panel A) changes from about ~150 nm for Al-free particles to 70 nm for Al-doped ones, in general agreement with the TEM data (Fig. 1). All the particles showed zeta potential in the range -40 mV to -30 mV that shifts in the negative direction with reducing the electrolyte concentration, and so the Debye length, in a series of washing steps (Fig. 6, B); this also affects the hydrodynamic size distribution via particle aggregation (Fig. 6, A). For SDS-capped particles, D_h magnitudes were almost the same but their zeta-potentials ranged from -20 mV to -35 mV (Fig. 6, D, E). The negative zeta-potentials for colloids both with and without SDS are almost independent of pH in the range of 3 to 11, with the dissolution yielding H_2S and covellite CuS started at pH < 3. This is surprising because brucite having the isoelectric point at pH ≥ 11 [72] should be charged positively in the pH region utilized here, and it is unlikely that the hydrophilic surface of valleriite is formed by sulfide sheets.

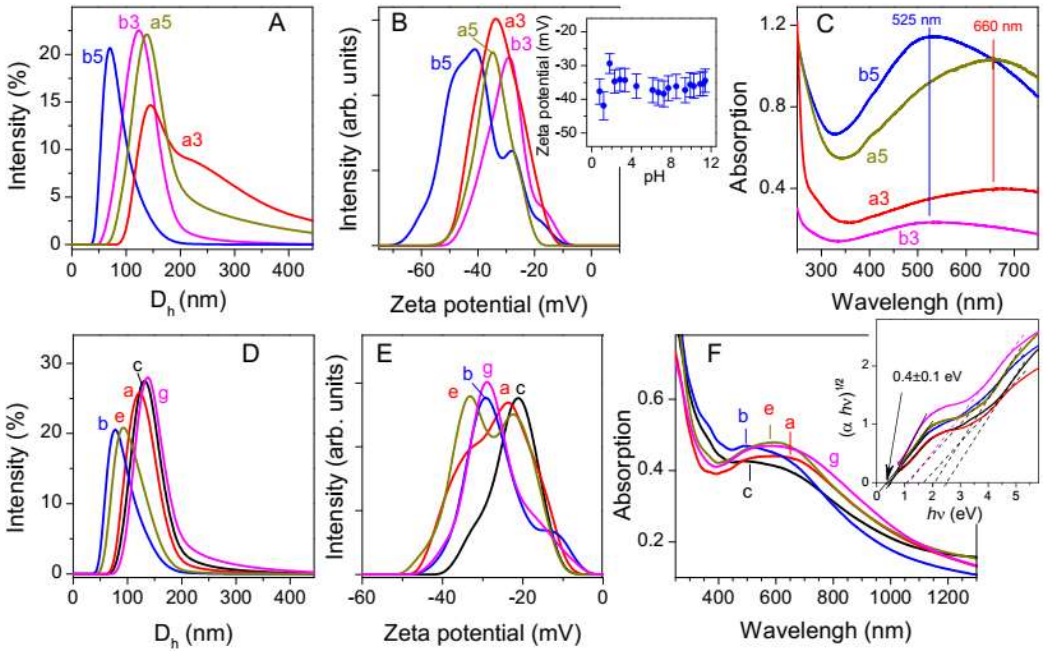

Fig. 6. The intensity distribution of the hydrodynamic diameter D_h (panels A, D), zeta potential (B, E) and UV-vis-NIR absorption spectra (C, F) of valleriite hydrosols spontaneously formed during washing (upper panels A-C and a zeta potential – pH plot for the sample b5 in an insert), and prepared by means of sonification of corresponding residues in aqueous 2 mM SDS solution (lower panels (D-F). In upper panels, the samples were synthesized (32 h) using the initial precursor ratios: a3, a5 - Al 0.5, Fe 2, Cu 2, Mg 2, S 14; b3, b5 - Al 0, Fe 2, Cu 2, Mg 2, S 14, with indexes 3 and 5 standing for the number of washing stage in which the particular sol was formed. In lower panels, hydrosol sample *a* contained no Al, b,c – Al-containing, e – Cr-doped, g – Co-doped (the designations are the same as in Table 1). pH 10.5±0.2, 25 °C.

UV-vis spectra (Fig. 6, panels C and F) show absorption maxima centered at ~520 nm (2.5 eV) for the particles containing Al (spectra b, c) and 600-700 nm (~2 eV) if no Al was added (curve a); the maxima are red-shifted for Cr- and Co-doped colloids despite the presence of Al (spectra e and g). The positions of maxima stay the same for various washing stages and for the relevant SDS-capped colloids, although their absorption intensities change with sol concentration. Analogous spectra with the absorption band at ~500 nm have been assigned to localized surface plasmon resonance (LSPR) for nanocrystals of chalcopyrite $CuFeS_2$ [73,74] albeit low free carrier densities in the semiconducting chalcogenides. Alternatively, and more likely, the UV-vis absorption is associated with a quasi-static dielectric resonance involving an intermediate band of empty Fe d-states [75-77]. It has been reported that the band shifts to larger wavelengths with decreasing content of Fe [77], and the NIR absorption for copper chalcogenides with no or low Fe was attributed to LSPR from electron holes in the VB related with Cu vacancies [77-79]. It is worth noting that the optical absorption energies for valleriite colloids coincide with the electron energy loss features at 2.0-2.5 eV in REELS (Fig. 3). Thus, the maxima seem to arise from the quasi-static dielectric resonance [75-77] due to the "intermediate" narrow minority-spin Fe 3d band (see the band scheme in Fig. 3). As demonstrated above, the more positive charge of the sulfide sheets induced by Al incorporation into hydroxide layers decreases the population of the minority-spin Fe 3d band, and probably slightly widens the VB-Fe3dβ gap. This is expected [76] to increase the quasi-static resonance energy, in agreement with the current experimental findings. On the other hand, the blue shift of the maxima may simply be due to the smaller size of the Al-doped particles (Fig. 1). The more complex electronic structures of Cr- and Co-doped valleriites require additional studies.

Tauc plots [80], which allow determining the band gap width, are presented in Fig. 6, F as the $(\alpha h\nu)^{1/2}$ vs $h\nu$ graphs for indirect band gap. The x-axis intersection points of the linear fit in the vis-NIR region give the band gap values of 0.4±0.1 eV for all the samples that correlates with the results of REELS. The high energy regions appear uninformative (the gap values varied from 1 to 3 eV) because overlapping the absorption maxima.

4. Discussion

The results on the synthesis and characterization of the valleriite-type materials obtained in this research are schematically summarized in Fig. 7 together with their prospective applications. The precursors spontaneously self-assemble into alternating quasi-atomic Cu-Fe-S sulfide and Mg hydroxide sheets in the hydrothermal process through a mechanism that still needs to be understood. The structure of valleriites formed by incommensurate 2D layers allows to vary widely, and to some extent independently, their composition and then properties, including replacement both of metals and chalcogenide atoms [30-34, 42-50]. On the other hand, the counterparts affect each other via the electric charges and probably other factors; this makes possible to finely adjust the material characteristics. Here, the ones were modified by changing the concentrations of Cu, Fe, Mg precursors and some modifiers and dopants as a first step toward fabrication and utilization of numerous new two-dimensional composites.

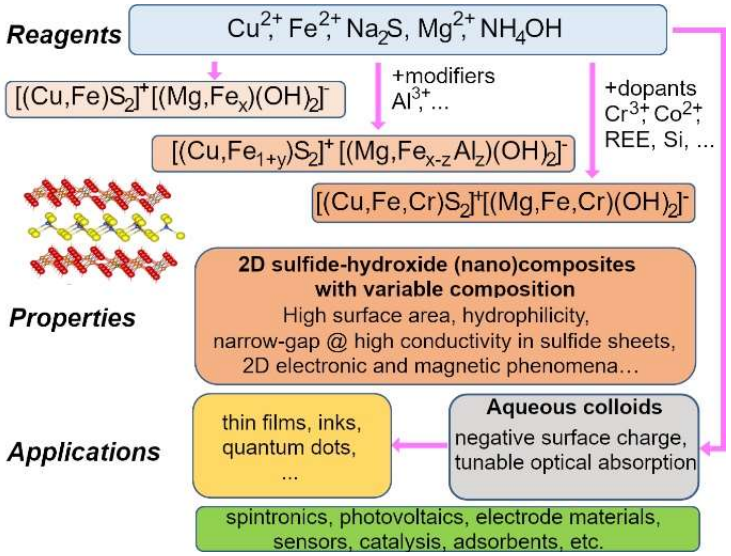

Fig. 7. Scheme illustrating the main factors influencing the preparation, composition and properties of valleriites as explored in this work, and their potential applications.

The current study revealed that the electronic, magnetic and optical characteristics of the valleriites are mainly determined by the metal sulfide component with the narrow forbidden band on the order of 0.4 eV, which depend on the electron density (electric charge) imposed by the hydroxide counterpart along with the metal (primarily Fe) vacancies, S-S bonding, transition metal doping, etc. The charge of the hydroxide layers can be controlled by the hydroxide counterpart via insertion of foreign elements (Al, Cr, and so on). It is accepted in the literature on natural valleriite that the hydroxide component carries a positive charge due to Al^{3+} and/or Fe^{3+} replacing Mg^{2+} cations. The above XPS and zeta potential measurements, however, imply the negative charge of hydroxide and the positive charge of sulfide sheets, probably as the excessive charge of trivalent cations is neutralized by O^{2-} species and additional OH^- anions attracted into the brucite-like structure. The more positive charge of sulfide layers leads, among other effects, to a reduced density of minority spins and an enhanced number of unpaired spins at Fe^{3+} sites, creating the large local hyperfine fields and peculiar magnetic properties of valleriite. The charges can be adjusted and probably reversed by incorporating, for example, monovalent cations akin to Li^+; this would allow to modify also the electronic and optical properties, including possible superconductivity [46-51].

The nanoscale valleriite particles form aqueous colloids, which show optical extinction tunable in the visible and NIR spectral region via the charge of sulfide layers and/or other factors, interesting for plasmonics, energy conversion, sensors and other applications. The phenomena may be rationalized in terms of quasi-static dielectric resonance [65-67], again with the participation of the minority-spin Fe 3d band. The colloids can be used as quantum dots and inks, precursors for deposition of thin films on various supports, and so on. The large surface area, layered structure, and specific chemical properties are essential for utilization of the nanoscale valleriites as adsorbents, catalysts, sensors, electrode materials, and so forth. The last but not the least is that the metal sulfide sheets embedded between hydroxide layers are more stable towards oxidation.

The valleriite-type materials with characteristics controllable through the chemical composition, size and morphology of the (nano)particles and other factors, emerge, therefore, as a new platform for 2D materials with a rich spectrum of potential applications comparable with graphene, transition metal dichalcogenides, MXens, layered double hydroxides. Certainly,

many problems regarding the formation mechanisms, structural, physical and chemical properties of the materials, still need to be investigated.

Conclusions

It is proposed a simple method of hydrothermal synthesis of valleriite particles (50-200 nm in the lateral size and 10-20 nm thick) composed of alternating 2D sheets of Cu-Fe sulfide and Mg-based hydroxide. The sulfide sheets close to $CuFeS_2$ composition contain Cu^+ and Fe^{3+} cations and monosulfide anions along with minor S-S species. XPS and Mössbauer spectroscopy found the content of ferric iron in hydroxide layers (10-45% of total Fe) can be reduced, in particular, by addition of Al. Valleriite was modified with transition 3d metals (Cr, Co) entering both sulfide and hydroxide layers, whereas only insignificant quantities of rare-earth elements and Si were uptaken. The electronic, optical and magnetic characteristics of the composites are largely determined by the sulfide component with the forbidden band gap of about 0.4 eV as derived from REELS and UV-vis-NIR spectra. At room temperature, Mössbauer spectra comprise of paramagnetic Fe signals in the sulfide and hydroxide layers, which transform to several Zeeman sextets due to magnetic ordering at 4.2 K, with the sextets with higher, up to 500 kOe, hyperfine magnetic fields originating from the sulfide layers with larger allocated positive charges. SQUID measurements revealed not pure paramagnetism but more complicated behavior for such samples, probably due to reduced population of minority-spin Fe 3d band. Raman spectra were found sensitive to Fe/Cu ratio in the sulfide layers. Colloidal solutions of valleriite, both formed spontaneously during the product washing and prepared by sonification of the precipitates in sodium dodecyl sulfate solutions, possess negative zeta potentials almost independent on pH, confirming a negative charge of hydroxide sheets, in agreement with the shifts of relevant photoelectron lines. UV-vis-NIR spectra show absorption maxima centered between ~500 nm and ~700 nm, whose energies coincide with the loss maxima at 2-2.5 eV in REELS, tentatively attributed to the quasi-static dielectric resonance involving “intermediate” empty Fe 3d band. Consequently, the nanoscale sulfide-hydroxide composites revealed a number of controllable electronic, magnetic, optical, interfacial properties interesting for many applications, thus defining a novel family of multifunctional two-dimensional materials.

Supplementary material

Scheme and photos of autoclave set-up (Fig. S1), additional TEM images (Fig. S2, S3), selected area electron diffraction patterns, elemental mapping (Fig. S3, S4), Mössbauer parameters (Table S1).

Acknowledgements

This research was supported by the Russian Science Foundation for Basic Research, Krasnoyarsk Territory Administration and Krasnoyarsk Territory Science Foundation, project 20-43-242903. Facilities of the Krasnoyarsk Regional Center of Research Equipment of Federal Research Center «Krasnoyarsk Science Center SB RAS» were employed in the work.

References

[1] S.K. Tiwari, S. Sahoo, N. Wang, A. Huczko, Graphene research and their outputs: status and prospect, J. Sci.: Adv. Mater. Devices 5 (2020) 10-29. https://doi.org/10.1016/j.jsamd.2020.01.006.

[2] A.K. Geim, I. V. Grigorieva, Van der Waals heterostructures, Nature 499 (2013) 419-425. https://doi.org/10.1038/nature12385.

[3] M. Xu, T. Lian, M. Shi, H. Chen, Graphene-like two-dimensional materials, Chem. Rev.113 (2013) 3766–3798. https://doi.org/10.1021/cr300263a.

[4] K. Zhang, Y. Feng, F. Wang, Z. Yang, J. Wang, Two dimensional hexagonal boron nitride (2D-hBN): synthesis, properties and applications, J. Mater. Chem. C 5 (2017) 11992−12022. https://doi.org/10.1039/C7TC04300G.
[5] K.S. Burch, D. Mandrus, J. Park, Magnetism in two-dimensional van der Waals materials, Nature 563 (2018) 47–52. https://doi.org/10.1038/s41586-018-0631-z.
[6] D.L. Cortie, G.L. Causer, K.C. Rule, H. Fritzsche, W. Kreuzpaintner, F. Klose, Two-dimensional magnets: forgotten history and recent progress towards spintronic applications, Adv. Funct. Mater. 30 (2019) 1901414. https://doi.org/10.1002/adfm.201901414.
[7] Y. Guo, S. Zhou, J. Zhao, Two-dimensional intrinsic ferromagnets with high Curie temperatures: Synthesis, physical properties and device applications, J. Mater. Chem. C 9 (2021) 6103-6121. https://doi.org/10.1039/D1TC00415H.
[8] Y.-W. Cheng, J.-H. Dai, Y.-M. Zhang, Y. Song, Two-dimensional, ordered, double transition metal carbides (MXenes): a new family of promising catalysts for the hydrogen evolution reaction, J. Phys. Chem. C 122 (2018) 28113-28122. https://doi.org/10.1021/acs.jpcc.8b08914.
[9] L. Verger, V. Natu, M. Carey, M.W. Barsoum, MXenes: an introduction of their synthesis, select properties, and applications, Trends Chem. 1 (2019) 656-669. https://doi.org/10.1016/j.trechm.2019.04.006.
[10] H. Kim, H. N. Alshareef, MXetronics: MXene-enabled electronic and photonic devices, ACS Materials Lett. 2 (2020) 55–70. https://doi.org/10.1021/acsmaterialslett.9b00419.
[11] M.-R. Gao, Y.-F. Xu, J. Jiang, S.-H. Yu, Nanostructured metal chalcogenides: synthesis, modification, and applications in energy conversion and storage devices, Chem. Soc. Rev. 42 (2013) 2986-3017. https://doi.org/10.1039/c2cs35310e.
[12] A.A. Tedstone, D.J. Lewis, P. O'Brien, Synthesis, properties, and applications of transition metal-doped layered transition metal dichalcogenides, Chem. Mater. 28 (2016) 1965-1974. https://doi.org/10.1021/acs.chemmater.6b00430.
[13] D. Monga, S. Sharma, N.P. Shetti, S. Basu, K.R. Reddy, T.M. Aminabhavi, Advances in transition metal dichalcogenide-based two-dimensional nanomaterials, Mater. Today Chem. 19 (2021) 100399. https://doi.org/10.1016/j.mtchem.2020.100399.
[14] Y. Li, Y. Wang, B. Pattengale, J. Yin, L. An, F. Cheng, Y. Li, J. Huang, P. Xi, High-index faceted $CuFeS_2$ nanosheets with enhanced behavior for boosting hydrogen evolution reaction, Nanoscale 2017, 9, 9230-9237. https://doi.org/10.1039/C7NR03182C.
[15] Z. Du, S. Yang, S. Li, J. Lou, S. Zhang, S. Wang, B. Li, Y. Gong, L. Song, X. Zou, P. M. Ajayan, Conversion of non-van der Waals solids to 2D transition-metal chalcogenides, Nature 577 (2020) 492-496. https://doi.org/10.1038/s41586-019-1904-x.
[16] T. Gao, Q. Zhang, L. Li, X. Zhou, L. Li, H. Li, T. Zhai, 2D ternary chalcogenides, Adv. Optical Mater. 6 (2018) 1800058. https://doi.org/10.1002/adom.201800058.
[17] Z. He, W. Que, Molybdenum disulfide nanomaterials: structures, properties, synthesis and recent progress on hydrogen evolution reaction, Appl. Mater. Today 3 (2016) 23-56. https://doi.org/10.1016/j.apmt.2016.02.001.
[18] R. Kumar, N. Goel, M. Hojamberdiev, M. Kumar, Transition metal dichalcogenides-based flexible gas sensors, Sens. Actuator. A Phys. 303 (2020) 111875. https://doi.org/10.1016/j.sna.2020.111875.
[19] S. Stolyarova, A. Kotsun, Y. Shubin, V. Koroteev, P. Plyusnin, Y. Mikhlin, M. Mel'gunov, A. Okotrub, L. Bulusheva, Synthesis of porous nanostructured MoS_2 materials in thermal shock conditions and their performance in lithium-ion batteries, ACS Appl. Energy Mater. 3 (2020) 10802–10813. https://doi.org/10.1021/acsaem.0c01837.
[20] H.T. Evans Jr., R. Allman, The crystal structure and crystal chemistry of valleriite, Z. fur Kristallogr. 127 (1968) 73-93. https://doi.org/10.1524/zkri.1968.127.1-4.73.

[21] A.D. Genkin, L.N. Val'sov, O valleriite i machinovite i usloviyakh ikh nakhozhdeniya v rudakh (On valleriite and Makhinovite and conditions of their presence in ores), Geol. Rud. Mestorozhd. 9 (1967) 94-106 (in Russian).
[22] L.J. Cabri, A new copper-iron sulfide, Econ. Geol. 62 (1967) 910-925. https://doi.org/10.2113/gsecongeo.62.7.910.
[23] D.C. Harris, D.J. Vaughan, Two fibrous iron sulfides and valleriite from Cyprus with new data on valleriite, Am. Mineral. 57 (1972) 1037–1052.
[24] N.I. Organova, Crystallochemistry of modulated and incommensurate structures in minerals, Int. Geol. Rev. 28 (1986) 802-814. https://doi.org/10.1080/00206818609466322.
[25] R. Li, L. Cui, Investigations on valleriite from Western China: crystal chemistry and separation properties, Int. J. Miner. Process. 41 (1994) 271-283. https://doi.org/10.1016/0301-7516(94)90033-7.
[26] F.B. Waanders, H. Pollak, Mössbauer spectroscopy to characterize iron sulphides, South Afr. J. Sci. 95 (1999) 387-390.
[27] A. Mücke, Review on mackinawite and valleriite: Formulae, localities, associations and intergrowths of the minerals, mode of formation and optical features in reflected light, J. Earth Sci. Clim. Change 8 (2017) 1000419. https://doi.org/10.4172/2157-7617.1000419.
[28] D.A. Dodin, Metallogeniya Taimyro-Noril'skogo regiona (Metallogeny of Taimyr-Noril'sk region), Nauka, St.-Petersburg, 2002 (in Russian).
[29] Yu.V. Laptev, V.S. Shevchenko, F.Kh. Urakaev, Sulphidation of valleriite in SO_2 solutions, Hydrometallurgy 98 (2009) 201–205. https://doi.org/10.1016/j.hydromet.2009.04.018.
[30] A.E. Hughes, G.A. Kakos, T.W. Turney, T.B. Williams, Synthesis and structure of valleriite, a layered metal hydroxide/sulfide composite, J. Solid State Chem. 104 (1993) 422-436. https://doi.org/10.1006/jssc.1993.1178.
[31] D.C. Harris, L.J. Cabri, J.M. Stewart, A "valleriite-type" mineral from Noril'sk, Western Siberia, Am. Mineral. 55 (1970) 2110-2114.
[32] I.V. Pekov, E.V. Sereda, V.O. Yapaskurt, Y.S. Polekhovsky, S.N. Britvin, N.V. Chukanov, Ferrovalleriite, $2(Fe,Cu)S \cdot 1.5Fe(OH)_2$: validation as a mineral species and new data, Geol. Ore Deposits 55 (2013) 637-647. https://doi.org/10.1134/S1075701513080102.
[33] E.H. Nickel, D.R. Hudson, The replacement of chrome spinel by chromian valleriite in sulphide-bearing ultramafic rocks in Western Australia, Contrib. Mineral. Petrol. 55 (1976) 265-277. https://doi.org/10.1007/BF00371337.
[34] I.V. Pekov, V.O. Yapaskurt, Y.S. Polekhovsky, M.F. Vigasina, O.I. Siidra, Ekplexite $(Nb,Mo)S_2 \cdot (Mg_{1-x}Al_x)(OH)_{2+x}$, kaskasite $(Mo,Nb)S_2 \cdot (Mg_{1-x}Al_x)(OH)_{2+x}$ and manganokaskasite $(Mo,Nb)S_2 \cdot (Mn_{1-x}Al_x)(OH)_{2+x}$, three new valleriite-group mineral species from the Khibiny alkaline complex, Kola Peninsula, Russia, Mineral. Mag. 78 (2014) 663–679. https://doi.org/10.1180/minmag.2014.078.3.14.
[35] N.I. Chistyakova, T.V. Gubaidulina, V.S. Rusakov, Mössbauer investigations of natural and synthetic tochilinite and valleriite, Czech. J. Phys. 56 (2006) E123–E131. https://doi.org/10.1007/s10582-006-0478-7.
[36] T.V. Gubaidulina, N.I. Chistyakova, V.S. Rusakov, Mössbauer study of layered iron hydroxysulfides: tochilinite and valleriite, Bull. Russ. Acad. Sci. Phys. 71 (2007) 1269–1272. https://doi.org/10.3103/S106287380709016X.
[37] N.I. Chistyakova, V.S. Rusakov, T.V. Gubaidulina, A.M. Gapochka, A.Yu. Bychkov, Mössbauer investigations of synthetic valleriite, Hyperfine Interact. 208 (2012) 99–104. https://doi.org/10.1007/s10751-011-0474-6.
[38] Y.L. Mikhlin, A.S. Romanchenko, E.V. Tomashevich, M.N. Volochaev, Yu.V. Laptev, XPS and XANES study of layered mineral valleriite, J. Struct. Chem. 58 (2017) 1137–1143. https://doi.org/10.1134/S0022476617060105.

[39] Y.L. Mikhlin, M.N. Likhatski, O.A. Bayukov, Y.V. Knyazev, D.A. Velikanov, Y.V. Tomashevich, A.S. Romanchenko, S.A. Vorobyev, M.V. Volochaev, S.M. Zharkov, D.M. Meira, Valleriite, a natural two-dimensional composite: X ray absorption, photoelectron and Mössbauer spectroscopy and magnetic characterization, ACS Omega 6 (2021) 7533–7543. http://dx.doi.org/10.1021/acsomega.0c06052.
[40] M. Borgheresi, F. Di Benedetto, M. Romanelli, M. Reissner, W. Lottermoser, R.R. Gainov, R.R. Khassanov, G. Tippelt, A. Giaccherini, L. Sorace, G. Montegrossi, R. Wagner, G. Amthauer, Mössbauer study of bornite and chemical bonding in Fe-bearing sulphides, Phys. Chem. Minerals 45 (2018) 227-235. https://doi.org/10.1007/s00269-017-0911-4.
[41] K. Iiishi, T. Tomisaka, T. Kato, S. Takeno, Syntheses of valleriite, Am. Mineral. 55 (1970) 2107-2110.
[42] S. Takeno, G.H. Moh, Syntheses of selenian valleriite, Mineral. Petrol. 50 (1994) 209-218. https://doi.org/10.1007/BF01164606.
[43] X.F. Lu, N.Z. Wang, H. Wu, Y.P. Wu, D. Zhao, X.Z. Zeng, X.G. Luo, T. Wu, W. Bao, G.H. Zhang, F.Q. Huang, Q.Z. Huang, X.H. Chen, Coexistence of superconductivity and antiferromagnetism in $(Li_{0.8}Fe_{0.2})OHFeSe$, Nature Mater. 14 (2015) 325–329. https://doi.org/10.1038/nmat4155.
[44] U. Pachmayr, F. Nitsche, H. Luetkens, S. Kamusella, F. Brückner, R. Sarkar, H.-H. Klauss, D. Johrendt, Coexistence of 3d-ferromagnetism and superconductivity in $[(Li_{1-x}Fe_x)OH](Fe_{1-y}Li_y)Se$, Angew. Chem. Int. Ed. 54 (2015) 293–297. https://doi.org/10.1002/anie.201407756.
[45] X. Dong, K. Jin, D. Yuan, H. Zhou, J. Yuan, Y. Huang, W. Hua, J. Sun, P. Zheng, W. Hu, Y. Mao, M. Ma, G. Zhang, F. Zhou, Z. Zhao, $(Li_{0.84}Fe_{0.16})OHFe_{0.98}Se$ superconductor: ion-exchange synthesis of large single-crystal and highly two-dimensional electron properties, Phys. Rev. B 92 (2015) 064515. https://doi.org/10.1103/PhysRevB.92.064515.
[46] D.N. Woodruff, F. Schild, C.V. Topping, S.J. Cassidy, J.N. Blandy, S.J. Blundell, A.L. Thompson, S.J. Clarke, The parent Li(OH)FeSe phase of lithium iron hydroxide selenide superconductors, Inorg. Chem. 55 (2016) 9886−9891. https://doi.org/10.1021/acs.inorgchem.6b01734.
[47] G.B. Hu, N.Z. Wang, M.Z. Shi, F.B. Meng, C. Shang, L.K. Ma, X.G. Luo, X.H. Chen, Superconductivity in solid-state synthesized (Li, Fe)OHFeSe by tuning Fe vacancies in FeSe layer, Phys. Rev. Mater. 3 (2019) 064802. https://doi.org/10.1103/PhysRevMaterials.3.064802.
[48] G. Hu, M. Shi, W. Wang, C. Zhu, Z. Sun, J. Cui, W. Zhuo, F. Yu, X. Luo, X. Chen, Superconductivity at 40 K in lithiation-processed $[(Fe,Al)(OH)_2][FeSe]_{1.2}$ with a layered structure, Inorg. Chem. 60 (2021) 3902−3908. https://dx.doi.org/10.1021/acs.inorgchem.0c03686
[49] U. Pachmayr, D. Johrendt, $[(Li_{0.8}Fe_{0.2})OH]FeS$ and the ferromagnetic superconductors $[(Li_{0.8}Fe_{0.2})OH]Fe(S_{1-x}Se_x)$, Chem. Commun. 51 (2015) 4689-4692. https://doi.org/10.1039/C5CC00038F.
[50] X. Zhou, C. Eckberg, B. Wilfong, S.-C. Liou, H. K. Vivanco, J. Paglione, E. E. Rodriguez, Superconductivity and magnetism in iron sulfides intercalated by metal hydroxides, Chem. Sci. 8 (2017) 3781–3788. https://doi.org/10.1039/c6sc05268a.
[51] A. Krzton-Maziopa, Intercalated iron chalcogenides: phase separation phenomena and superconducting properties, Front. Chem. 9 (2021) 640361. https://doi.org/10.3389/fchem.2021.640361.
[52] R.V. Borisov, O.V. Belousov, A.M. Zhizhaev, Synthesis of Pd, Pt and Pd–Pt nanoparticles on carbon nanotubes under hydrothermal autoclave conditions, Russ. J. Inorg. Chem. 65 (2020) 1623–1629. https://doi.org/10.1134/S0036023620100034.

[53] A.P. Grosvenor, B.A. Kobe, M.C. Biesinger, N.S. McIntyre, Investigation of multiplet splitting of Fe 2p XPS spectra and bonding in iron compounds, Surf. Interface Anal. 36 (2004) 1564-1574. https://doi.org/10.1002/sia.1984.
[54] A.M. Sazonov, S.A. Silyanov, O.A. Bayukov, Y.V. Knyazev, Y.A. Zvyagina, P.A. Tishin, Composition and ligand microstructure of arsenopyrite from gold ore deposits of the Yenisei Ridge (Eastern Siberia, Russia), Minerals 9 (2019) 737. https://doi.org/10.3390/min9120737.
[55] D.A. Velikanov, High-sensitivity measurements of the magnetic properties of materials at cryogenic temperatures, Inorg. Mater. Appl. Res. 11 (2020) 801–808. https://doi.org/10.1134/S2075113320040413.
[56] S. Goh, A. Buckley, R. Lamb, R. Rosenberg, D. Moran, The oxidation states of copper and iron in mineral sulfides, and the oxides formed on initial exposure of chalcopyrite and bornite to air, Geochim. Cosmochim. Acta 70 (2006) 2210–2228. https://doi.org/10.1016/j.gca.2006.02.007.
[57] Y. Mikhlin, V. Nasluzov, A. Ivaneeva, S. Vorobyev, M. Likhatski, A. Romanchenko, A. Krylov, S. Zharkov, D. M. Meira, Formation, evolution and characteristics of copper sulfide nanoparticles in the reactions of aqueous cupric and sulfide ions, Mater. Chem. Phys. 255 (2020) 123600. https://doi.org/10.1016/j.matchemphys.2020.123600.
[58] Y. Mikhlin, V. Nasluzov, A. Romanchenko, Y. Tomashevich, A. Shor, R. Felix, Layered structure of the near-surface region of oxidized chalcopyrite ($CuFeS_2$): hard X-ray photoelectron spectroscopy, X-ray absorption spectroscopy and DFT+U studies, Phys. Chem. Chem. Phys. 19 (2017) 2749 – 2759. https://doi.org/10.1039/C6CP07598C.
[59] V. Nasluzov, A. Shor, A. Romanchenko, Y. Tomashevich, Y. Mikhlin, DFT + U and low-temperature XPS studies of Fe-depleted chalcopyrite ($CuFeS_2$) surfaces: a focus on polysulfide species, J. Phys. Chem. C 123 (2019) 21031–21041. https://doi.org/10.1021/acs.jpcc.9b06127.
[60] Y. Mikhlin, A. Romanchenko, Y. Tomashevich, Surface and interface analysis of iron sulfides in aqueous media using X-ray photoelectron spectroscopy of fast-frozen dispersions, Appl. Surf. Sci.549 (2021) 149261. https://doi.org/10.1016/j.apsusc.2021.149261.
[61] M. Vos, S.W. King, B.L. French, Measurement of the band gap by reflection electron energy loss spectroscopy, J. Electron Spectrosc. Rel. Phenom. 212 (2016) 74–80. http://dx.doi.org/10.1016/j.elspec.2016.08.001.
[62] C. Richter, B.A. van der Pluijm, Separation of paramagnetic and ferrimagnetic susceptibilities using low temperature magnetic susceptibilities and comparison with high field methods, Phys. Earth Planet. Inter. 83 (1994) 113—123. https://doi.org/10.1016/0031-9201(94)90084-1.
[63] D. Peddis, D. Rinaldi, G. Ennas, A. Scano, E. Agostinelli, D. Fiorani, Superparamagnetic blocking and superspin-glass freezing in ultra small δ-($Fe_{0.67}Mn_{0.33}$)OOH particles, Phys. Chem. Chem. Phys. 14 (2012) 3162–3169. https://doi.org/10.1039/C2CP22473A.
[64] J.L. Dormann, R. Cherkaoui, L. Spinu, M. Noguès, F. Lucari, F. D'Orazio, D. Fiorani, A. Garcia, E. Tronc, J.P. Jovilet, From pure superparamagnetic regime to glass collective state of magnetic moments in γ-Fe_2O_3 nanoparticle assemblies, J. Magn. Magn. Mater. 187 (1998) L139-L144. https://doi.org/10.1016/S0304-8853(98)00135-8
[65] J. Navrátil, P. Levinský, J. Hejtmánek, M. Pashchenko, K. Knížek, L. Kubícková, T. Kmjec, C. Drašar, Peculiar magnetic and transport properties of $CuFeS_2$: defects play a key role, J. Phys. Chem. C 124 (2020) 20773−20783. https://dx.doi.org/10.1021/acs.jpcc.0c06490.
[66] X. Zhang, Q.-H. Tan, J.-B. Wu, W. Shi, P.-H. Tan, Review on the Raman spectroscopy of different types of layered materials, Nanoscale 8 (2016) 6435–6450. https://doi.org/10.1039/c5nr07205k.

[67] https://rruff.info/valleriite/names/asc/R080119.
[68] https://rruff.info/chalcopyrite/names/asc/R050018.
[69] G.K. Parker, R. Woods, G.A. Hope, Raman investigation of chalcopyrite oxidation, Colloids Surf. Physicochem. Eng. Asp. 318 (2008) 160–168. https://doi.org/10.1016/j.colsurfa.2007.12.030.
[70] S.N. White, Laser Raman spectroscopy as a technique for identification of seafloor hydrothermal and cold seep minerals, Chem. Geol. 259 (2009) 240–252. https://doi.org/10.1016/j.chemgeo.2008.11.008.
[71] F.W. Ohrendorf, H. Haeuseler, Lattice dynamics of chalcopyrite type compounds. Part I. Vibrational frequencies, Cryst. Res. Technol. 34 (1999) 339–349. https://doi.org/10.1002/(SICI)1521-4079(199903)34:3%3C339::AID-CRAT339%3E3.0.CO;2-E
[72] M. Kosmulski, Isoelectric points and points of zero charge of metal (hydr)oxides: 50 years after Parks' review, Adv. Colloid Interf. Sci. 238 (2016) 1–61. https://doi.org/10.1016/j.cis.2016.10.005.
[73] B. Bhattacharyya, A. Pandey, $CuFeS_2$ quantum dots and highly luminescent $CuFeS_2$ based core/shell structures: Synthesis, tunability, and photophysics, J. Am. Chem. Soc. 138 (2016) 10207-10213. https://doi.org/10.1021/jacs.6b04981.
[74] G. Gabka, P. Bujak, A. Ostrowski, W. Tomaszewski, W. Lisowski, J.W. Sobczak, A. Pron, Cu-Fe-S nanocrystals exhibiting tunable localized surface plasmon resonance in the visible to NIR spectral ranges, Inorg. Chem. 55 (2016) 6660−6669. https://doi.org/10.1021/acs.inorgchem.6b00912.
[75] S. Ghosh, T. Avellini, A. Petrelli, I. Kriegel, R. Gaspari, G. Almeida, G. Bertoni, A. Cavalli, F. Scotognella, T. Pellegrino, L. Manna, Colloidal $CuFeS_2$ nanocrystals: intermediate Fe d-band leads to high photothermal conversion efficiency, Chem. Mater. 28 (2016) 4848-4858. https://doi.org/10.1021/acs.chemmater.6b02192.
[76] R. Gaspari, G. Della Valle, S. Ghosh, I. Kriegel, F. Scotognella, A. Cavalli, L. Manna, Quasi-static resonances in the visible Spectrum from all-dielectric intermediate band semiconductor nanocrystals, Nano Lett. 17 (2017) 7691−7695. https://doi.org10.1021/acs.nanolett.7b03787.
[77] S. Lee, S. Ghosh, C. E. Hoyer, H. Liu, X. Li, V.C. Holmberg, Iron-content-dependent, quasi-static dielectric resonances and oxidative transitions in bornite and chalcopyrite copper iron sulfide nanocrystals, Chem. Mater. 33 (2021) 1821–1831. https://doi.org/10.1021/acs.chemmater.0c04798.
[78] A. Agrawal, S.H. Cho, O. Zandi, S. Ghosh, R.W. Johns, D.J. Milliron, Localized surface plasmon resonance in semiconductor nanocrystals, Chem. Rev. 118 (2018) 3121−3207. https://doi.org/10.1021/acs.chemrev.7b00613.
[79] W. van der Stam, S. Gudjonsdottir, W.H. Evers, A.J. Houtepen, Switching between plasmonic and fluorescent copper sulfide nanocrystals, J. Am. Chem. Soc.139 (2017) 13208−13217. https://doi.org/10.1021/jacs.7b07788.
[80] J. Tauc, Optical properties and electronic structure of amorphous Ge and Si, Mater. Res. Bull. 3 (1968) 37-46. https://doi.org/10.1016/0025-5408(68)90023-8.